SPACE TELESCOPE SCIENCE INSTITUTE
Operated for NASA by AURA

Instrument Science Report WFC3 2009-03

WFC3 TV3 Testing: UVIS-1' Crosstalk

S.Baggett
May 6, 2009

ABSTRACT

This report summarizes the behavior of the crosstalk in the Wide Field Camera 3 UVIS-1' flight detector based on thermal-vacuum data taken with the integrated instrument. A non-linear type of crosstalk seen in previous tests, where a target in one quadrant gives rise to a significant mirror image in each of the other three quadrants, is confirmed as gone (<0.1 e^-), thanks to a hardware fix to the CCD electronics box and a new timing pattern. A small amount of crosstalk remains, in which point sources, extended targets, hot pixels, and cosmic rays generate a low-level mirror image in the quadrant adjoining the target quadrant, on the same chip. This residual crosstalk is linear, negative, and appears at the level of ~10^{-4} to 10^{-5} in unbinned, nominal gain (1.5 e^-/DN), full-frame 4-amp readouts; the higher level occurs for targets imaged in quadrants A or C and the lower level for targets placed in quadrants B or D. In 3x3 binned 4-amp readouts, the crosstalk from point source targets placed in D is about 20% higher than that seen in unbinned readout. However, the crosstalk in binned frames is negligible for targets placed in quadrants A and B and only a small amount of crosstalk (~5x10^{-5}) occurs due targets placed in C quadrant.

Introduction

Images taken with the integrated WFC3 instrument in early 2004 under ambient conditions and in late 2004 under thermal vacuum conditions revealed the presence of crosstalk (CT): a light source in one quadrant of the field of view generating low level electronic mirror images in one or more other quadrants. This phenomenon was not completely unexpected, as it frequently occurs whenever two or more channels are read out

simultaneously (Janesick, 2001). The CT in WFC3 as characterized during those early tests has been discussed in previous reports (Baggett et al., 2004; Baggett et al., 2005) and can be summarized briefly as follows. Two types of crosstalk were initially identified: 1) sources at any exposure level in any quadrant caused highly non-linear CT in the three other quadrants and 2) pixels in any quadrant caused low-level CT in the adjoining quadrant, i.e., on the same CCD chip. The first type of CT produced mirror-image features at relatively low levels (~15 e^- at gain 1.5) regardless of the source exposure level. Changing bias levels and gain settings caused changes to the sign, and to some extent, the magnitude of the CT, implying that the crosstalk-inducing signal was somewhere within or following the gain stage. In addition, the CT varied as a function of the binning and number of amps used during the image readout: full-frame images that were binned (either 2x2 or 3x3) and read out with only 2 amps exhibited no crosstalk at all; full-frame images that were binned and read out with 4 amps exhibited only the second type of CT (same chip, i.e., on amp adjacent to the target amp). The second type of CT was initially attributed to saturated pixels only but has since been found to be present at a low level at all exposure levels and is the subject of this report.

Following the observations of the two types of crosstalk, modelling of the electronics and testing with the non-flight CCD electronics box (CEB) at the GSFC Detector Characterization Lab revealed that there was a common-mode susceptibility in the CEB and that adding a balancing capacitor would partially reduce the CT levels. In addition, the timing pattern in use at the time was found to be a contributing factor: the digitization of pixels by the A/D converter could interfere with the analog sampling of the subsequent pixels, thereby injecting CT. This hypothesis was consistent with the lack of CT in 2-amp binned images (Baggett et al., 2004) and confirmed via images taken with the A/D conversion speed doubled: the CT could be alleviated by compressing and shifting the sample time away from the A/D timing. As a consequence, a new timing pattern was developed and is now in use.

With these hardware and timing pattern changes in place, the UVIS-1' detector package integrated into WFC3 underwent further thermal vacuum testing in the spring of 2008 (thermal vacuum ground test 3, TV3). This report summarizes the behavior of the residual WFC3 UVIS crosstalk in light of the modifications.

Data

The results discussed here are based on a variety of data taken during the last thermal vacuum test. First, two programs specifically aimed at investigating crosstalk were executed. The first test was performed on Feb 28, 2008, with the detector at the off-nominal temperature of about -50C. A set of 3 images were taken in each of the 4 quadrants: a HeNe point source with peak level ~30K e^-, an extended point source using the 200μ VISIR target with peak level ~50K e^-, and finally, another HeNe point source that was

deliberately saturated to ~100x the level of the first image. The second program was run on March 11, 2008, with the detector at the nominal operating temperature of ~-83 C. In this case, a set of 6 images were acquired on each quadrant with the extended 200μ VISIR point source. The first four images in each quadrant were taken at the nominal focus setting, tuned to achieve peak levels of ~9K, 23K, 37K, and 50K e^- . The last two images of each set were taken with the optical stimulus at -15mm defocus setting in order to spread the light out even farther; peak exposure levels were ~8K e^- and ~45K e^- . In all cases, images were full-frame, unbinned, four-amp read outs taken at the nominal gain setting (1.5 e^-/DN); an example of one of the full-frame images is shown in Figure 1. All the images from the two crosstalk tests are tabulated in Appendix A; a mosaic of the targets and the corresponding crosstalk are include in Appendix B (Figure 4 and Figure 5).

Finally, data from two other proposals, while not obtained specifically for the purpose of investigating crosstalk, have been included in the analysis as well: the long exposure-time, full-frame UVIS dark frames (iu01* series) and the UVIS "glint" frames (iu26* series). The former are used here to evaluate the behavior of CT due to hot pixels and cosmic rays while the latter, taken in 3x3 binned mode as part of a program to search for residual scattered light, are used to quantify CT behavior in binned frames. All the images from these two tests are tabulated in Appendix A as well; mosaics of some of the binned frames are in Appendix B (Figure 6).

Figure 1: At left, a typical crosstalk test image, shown with a hard inverted greyscale stretch. In this case, the extended 200μ point source target was placed in quadrant C, using -15mm defocus, and the crosstalk appears in quadrant D. The faint large ring in C offset from the primary target is an optical ghost due to reflection between the detector window and filter. The right plot shows a 20 line average cut through the target and through the crosstalk (after each quadrant is aligned so the readouts are in the same direction); the logarithmic yaxis is in units of electrons.

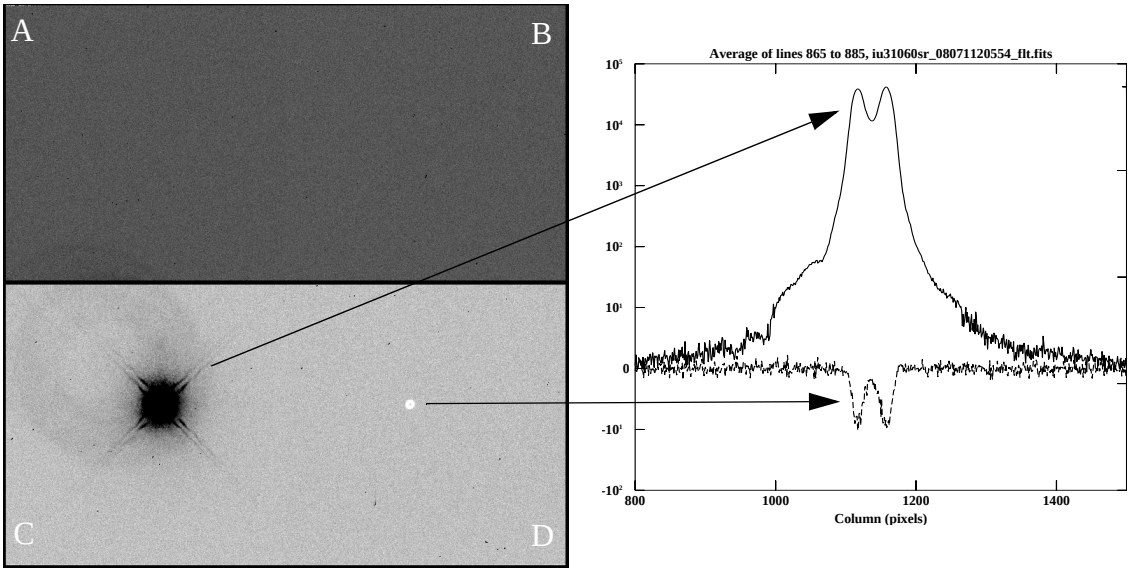

Analysis

Each full-frame, four-amp image containing a target was searched for any evidence of CT, both visually and quantitatively. The images were first fully calibrated using calwf3 and the best available reference files. The full-frame images were then split into four separate images, one for each quadrant, with the images rotated/flipped as necessary such that the read out directions all aligned with that of quadrant A.

Figure 5 in Appendix B presents an image mosaic of 100x100 pixels subsections of the data taken as part of the first crosstalk proposal, with the detector at ambient. Pairs of columns show sections extracted from the full-frame images: columns 1 and 2 are from images where the target was placed in quadrant A (col 1) and crosstalk appeared in quadrant B (col 2). Similarly, columns 3 and 4 are from images where the target was placed in quadant B and crosstalk appeared in quadrant A (col 4), and so on. The HeNe laser was used to generate an unsaturated point source target (peak level ~30K e^-) in the first row images and 100x that exposure level in the third row images. Images in the middle row contain a more extended source (200μ fiber), with exposure level just at saturation. The CT is apparent only for the more heavily-exposed targets and is clearly worse when the target is in quadrant A or C than when the target is in B or D.

Figure 4 in Appendix B contains a mosaic of image subsections from part of the second crosstalk proposal, with the detector at its nominal operating temperature. The odd columns show the target in quadrants A, B, C, and D while the even columns show the respective mirror images in the adjacent quadrant (i.e., B, A, D, and C, respectively). The rows contain data at different exposure and/or focus settings; the exposure level increases from row 1 through 4; the last two rows show defocussed images at two different exposure levels. Again, the CT appears worst when the target is placed in quadrants A or C.

To quantify the effect, linear fits were made to the pixel values from the target amp as a function of their value in the victim amp. Figure 2 illustrates two of the resulting plots and fits; individual points represent each pixel while the large triangles show the averages across 1000e^- wide bins. At left is the case where a target is placed in quadrant D and CT arises in C; at right, the target is in C and CT in D. Fits for point source or extended targets were performed on image subsections, typically 100x100 or 200x200 pixels in size, while the hot pixel/cosmic ray fits were done on all pixels with level higher than 20e^- within the target quadrant. To minimize degradation of the fits from cosmic rays or hot pixels within the victim quadrant, the victim pixel values were limited to +/-20 e^-.

Figure 2: Comparison of point source pixel values in the target quadrant versus victim quadrant along with the resultant linear fit. The large triangles are averages over bins 1000e$^-$ in width. The point source target was placed in quadrant D and C in the left and right plots, respectively, with crosstalk in C and D.

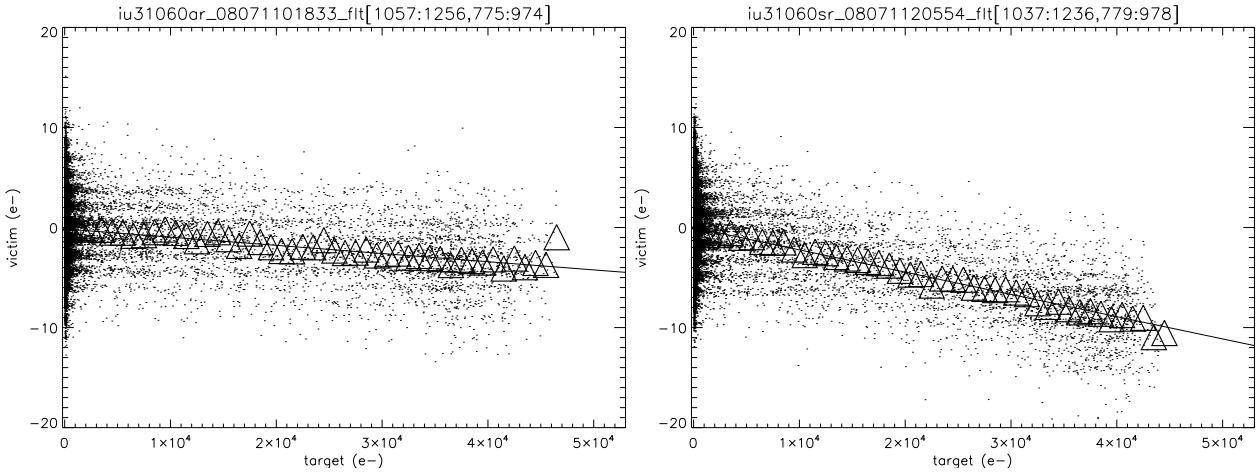

This fitting procedure was performed on all crosstalk images and the resulting linear fits were used to compute the level of crosstalk at a fiducial point of 50,000 e$^-$. The results from all fits have been summarized in Table 1 for the various datasets outlined earlier: the crosstalk data with the detector at ambient and nominal operating temperatures as well as the glint data (binned 3x3) and the darks taken at the nominal detector temperature. Each table row lists the amp in which the target had been placed, whether all pixels or only unsaturated pixels were used in the fit, the number of images in the set, the mean CT level at 50K e$^-$, the error in the mean CT level, as well as the max, min, and median CT levels. Visually, there did not appear to be any CT in each of the quadrants on the chip other than the target chip; fits to the target pixels vs each of the other quadrants, tabulated in Table 2, confirmed that conclusion.

The results of the fitting and image evaluations can be summarized as follows.

1. The CT levels are about $2x10^{-4}$ when the target is in quadrants A or C and about $8x10^{-5}$ when the target is in B or D.

2. The quadrants on the chip other than the chip containing the target show no evidence for CT.

3. To within the errors, the CT due to hot pixels and cosmic rays is the same as that due to point or extended sources.

4. The CT levels are somewhat higher at the nominal operating temperature than when the detector is warmer though the error bars on the latter are also higher, attributed to the increased noise from operating at a higher temperature.

5. The binned data exhibited mixed CT results. While targets placed in quadrants A or B show no evidence of CT, targets placed in C contained considerably less CT (~$5x10^{-5}$) than the unbinned frames (~$2x10^{-4}$) while the CT due to targets placed in D is a bit worse in binned data (~$1.2x10^{-4}$) than in unbinned data (~$9.2x10^{-5}$). The reason for this is unclear as the same type of point source was used in all quadrants. More data acquired on-orbit may help to shed more light on this issue.

The resulting fits were used to correct two images from the crosstalk proposals, one extended and one point source target taken at the nominal and ambient operating temperatures, respectively. The appropriate linear fit was applied to the target quadrant and subtracted from the victim quadrant. The average fit sufficed for correcting the nominal temperature data but due to the noisier CT results from the ambient temperature images, it was necessary to use the median fit to obtain an adequate removal of the CT. The results are shown in Figure 3, where the image subsections and average slices through the corrected image show that the CT removal was quite effective: there is no trace of CT after the correction and no apparent change in noise characteristics.

Table 1. Crosstalk levels at 50Ke^- in the quadrant adjacent to the quadrant containing the target.

target quadrant	pixels	num images	mean CT at 50K e^-	CT error	CT max	CT min	CT median
Ambient operating temperature, unbinned							
a	all	3	-8.16	1.16	-5.30	-9.71	-9.47
a	nosat	3	-7.93	1.16	-5.30	-9.47	-9.01
b	all	3	-0.68	1.21	1.82	-2.19	-1.67
b	nosat	3	-0.77	1.22	1.82	-2.46	-1.67
c	all	3	-10.21	1.24	-10.02	-10.44	-10.18
c	nosat	3	-10.31	1.25	-10.18	-10.44	-10.31
d	all	3	-3.69	1.26	-3.21	-4.50	-3.36
d	nosat	3	-3.96	1.28	-3.36	-4.50	-4.00
Nominal operating temperature, unbinned							
a	all	6	-10.24	0.27	-9.37	-10.92	-10.39
a	nosat	6	-10.24	0.27	-9.37	-10.92	-10.39
b	all	6	-3.08	0.25	-1.87	-4.59	-3.03
b	nosat	6	-3.08	0.25	-1.87	-4.59	-3.03
c	all	6	-11.04	0.26	-10.18	-11.53	-11.05

target quadrant	pixels	num images	mean CT at 50K e^-	CT error	CT max	CT min	CT median
c	nosat	6	-11.04	0.26	-10.18	-11.53	-11.05
d	all	6	-4.63	0.26	-4.04	-5.99	-4.42
d	nosat	6	-4.63	0.26	-4.04	-5.99	-4.42
Nominal operating temperature, binned							
a	all	16	0.04	0.08	0.50	-0.52	0.11
a	nosat	16	0.04	0.08	0.50	-0.52	0.11
b	all	16	0.02	0.09	1.05	-0.82	-0.09
b	nosat	16	0.02	0.09	1.05	-0.82	-0.09
c	all	16	-2.11	0.09	-1.42	-3.28	-2.08
c	nosat	16	-3.48	0.36	-1.13	-9.30	-2.79
d	all	16	-5.81	0.08	-5.32	-6.47	-5.86
d	nosat	16	-5.89	0.39	-1.99	-8.62	-5.99
Nominal operating temperature, unbinned, hotpixels							
a	all	6	-10.34	0.20	-9.51	-10.79	-10.55
a	nosat	6	-10.65	0.39	-10.09	-11.26	-10.69
b	all	6	-3.23	0.18	-2.21	-4.07	-3.39
b	nosat	6	-3.52	0.41	-1.27	-5.36	-3.38
c	all	6	-12.13	0.89	-10.22	-15.22	-11.71
c	nosat	6	-12.84	0.94	-11.67	-15.22	-12.50
d	all	6	-4.03	1.14	1.08	-7.31	-4.56
d	nosat	6	-3.91	1.16	1.08	-7.31	-4.65

Table 2. Mean crosstalk level at 50K e^- in quadrants on the chip *other* than target chip.

target quadrant	CT quad	pixels	num images	mean CT at 50K e^-	CT error	CT max	CT min	CT median
Ambient operating temperature, unbinned								
a	quad1	all	3	-0.87	1.18	-0.01	-2.26	-0.35
a	quad2	all	3	0.08	1.15	0.95	-0.39	-0.32
b	quad1	all	3	-0.30	1.21	0.07	-0.55	-0.41
b	quad2	all	3	1.48	1.19	4.55	-0.17	0.06
c	quad1	all	3	0.21	1.23	0.76	-0.08	-0.04

target quadrant	CT quad	pixels	num images	mean CT at 50K e^-	CT error	CT max	CT min	CT median
c	quad2	all	3	1.79	5.80	-0.43	-0.01	3.48
d	quad1	all	3	-0.08	1.20	0.15	-0.39	0.01
d	quad2	all	3	-0.09	1.26	0.01	-0.25	-0.04
Nominal operating temperature, unbinned								
a	quad1	all	6	-0.05	0.27	0.37	-0.55	0.05
a	quad2	all	6	0.20	0.27	1.00	-0.28	0.13
b	quad1	all	6	-0.12	0.26	0.12	-0.50	-0.05
b	quad2	all	6	0.28	0.26	0.80	0.13	0.19
c	quad1	all	6	-0.34	0.25	0.20	-1.21	-0.32
c	quad2	all	6	0.07	0.26	1.59	-1.23	0.10
d	quad1	all	6	-0.44	0.25	0.08	-0.96	-0.48
d	quad2	all	6	0.02	0.26	0.18	-0.08	-0.01
Nominal operating temperature, binned								
a	quad1	all	16	0.04	0.08	0.60	-0.42	-0.01
a	quad2	all	16	-0.07	0.09	0.81	-1.08	-0.06
b	quad1	all	16	0.03	0.09	0.46	-0.61	0.04
b	quad2	all	16	0.07	0.09	0.74	-0.63	0.09
c	quad1	all	16	0.14	0.09	0.93	-0.56	0.17
c	quad2	all	16	0.17	0.09	0.96	-0.57	0.18
d	quad1	all	16	0.18	0.08	0.70	-0.28	0.22
d	quad2	all	16	-0.00	0.08	0.94	-0.70	-0.02

Figure 3: Correction of crosstalk in a nominal-temperature, extended target image and an ambient-temperature point source target. Images are shown with a hard, inverted stretch; with the target, CT, and corrected images in columns 1,2, and 3, respectively. Plots at right show image slices of the CT before and after the correction (solid and dashed lines).

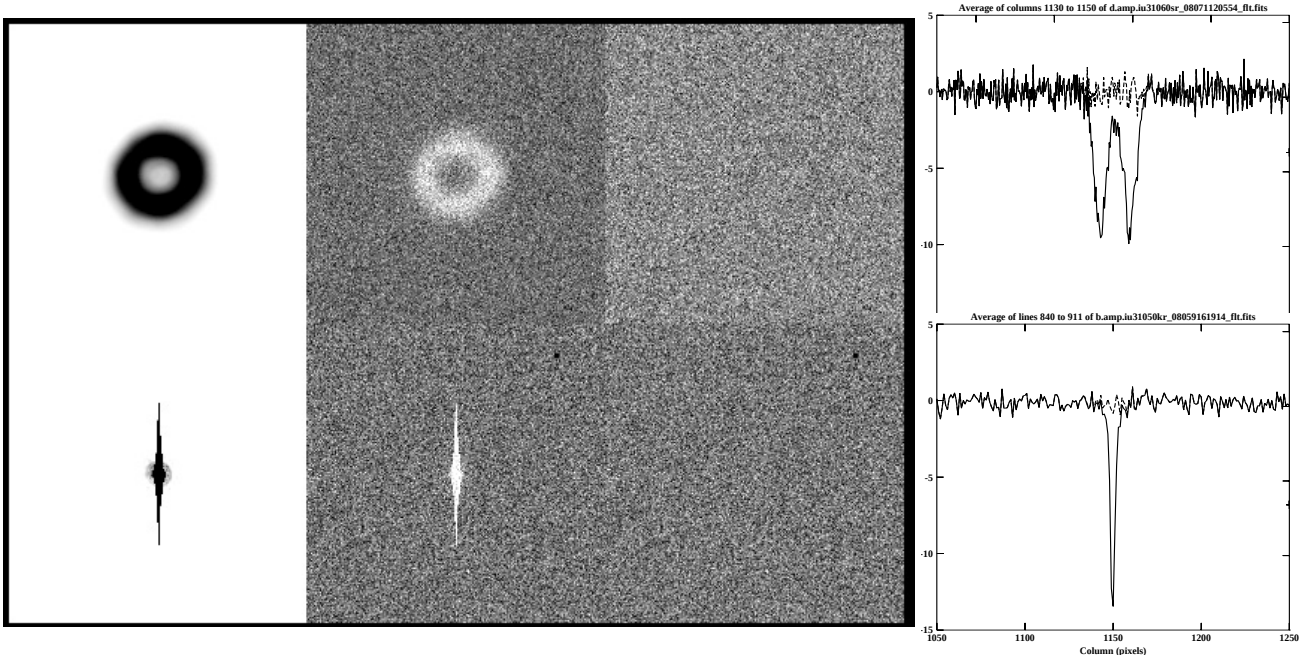

Conclusions

While the extended, highly non-linear crosstalk has been eliminated from the UVIS-1' detector and there is no more crosstalk (CT) between the two chips, a low level of crosstalk within a given chip remains. The CT appears only in the amp adjacent to the amp containing the target, at ~10^{-4} level for targets placed in quadrants A or C and somewhat less for targets placed in quadrants B or D (~10^{-5}). Hot pixels and cosmic rays exhibit CT at the same level as the point and extended sources; binned data appear to have less CT overall with the exception of quadrant D. The CT in the relatively simple ground test data, with a single source in one quadrant, was easily eliminated via the use of an appropriate linear fit. Application of this technique to on-orbit data, with targets present simultaneously in all four quadrants, will likely require some refinements to the procedure, such as performing the corrections iteratively or applying the correction only to target pixel values exceeding a certain threshold.

Acknowledgements

Thanks are due to the extended WFC3 team who supported the ground tests and thanks to Peter McCullough, George Hartig, John MacKenty, Randy Kimble, and Howard Bushouse for helpful discussions.

References

S.Baggett, G.Hartig, E.Cheung, “WFC3 UVIS Crosstalk Images,” WFC3 Instrument Science Report 2004-11, July 2004.

S. Baggett, R. Hill, G. Hartig, A. Waczynski, Y. Wen, “WFC3 Thermal Vacuum Testing: UVIS Crosstalk,” WFC3 Instrument Science Report 2005-05, Feb 2005.

Janesick, James R., “Scientific Charge-Coupled Devices,” SPIE Press, Bellingham, WA, 2001.

Appendix A

Summary of ground test observations examined for crosstalk. Listed are the image identfication number from the ground test database, image name, exposure time, observation date and time, stimulus source (HeNe laser or 200um point source), field point and quadrant location of target. The comment field records either the approximate peak pixel level in e^- or indication of whether the image was saturated or taken at a defocus setting. All images are four-amp readouts, taken with the F625W filter, at the nominal gain 1.5 setting, default bias offset level, and on side 1 (MEB1) of the instrument. The iu3105* series were taken with the detector warm, at about -50C, while the iu3106*, iu01*, and iu26* series were taken with the detector at the nominal cold temperature, about -83 C. Due to the large number of images in the latter set, only the first and last images of the series have been listed.

tvnum	image	exptime	date-obs	time-obs	source	field point	quadrant	comment
49158	iu310501r_08059142437	10.0	2008-02-28	14:22:03.04	HeNe	UV13	D	30K
49159	iu310503r_08059143705	12.5	2008-02-28	14:34:28.06	VISIR200	UV13	D	50K
49160	iu310505r_08059144852	10.0	2008-02-28	14:46:18.05	HeNe	UV13	D	saturated
49161	iu310507r_08059145934	10.0	2008-02-28	14:57:00.06	HeNe	UV14	B	27K
49162	iu310509r_08059151705	12.5	2008-02-28	15:08:40.06	VISIR200	UV14	B	50K
49163	iu31050ar_08059151705	10.0	2008-02-28	15:14:25.06	HeNe	UV14	B	saturated
49164	iu31050cr_08059153040	10.0	2008-02-28	15:28:06.05	HeNe	UV15	C	29K
49165	iu31050er_08059154811	12.5	2008-02-28	15:39:46.05	VISIR200	UV15	C	51K
49166	iu31050fr_08059154811	10.0	2008-02-28	15:45:31.04	HeNe	UV15	C	saturated
49167	iu31050hr_08059160146	10.0	2008-02-28	15:59:12.06	HeNe	UV16	A	28K
49168	iu31050jr_08059161914	12.5	2008-02-28	16:10:53.06	VISIR200	UV16	A	50 K
49169	iu31050kr_08059161914	10.0	2008-02-28	16:16:38.06	HeNe	UV16	A	saturated
49170	iu31050mr_08059163336	0.0	2008-02-28	16:30:24.06	--	--	--	bias
50817	iu310601r_08071092452	0.0	2008-03-11	09:19:24.04	--	--	--	bias
50818	iu310602r_08071092452	2.6	2008-03-11	09:22:25.06	VISIR200	UV13	D	9K
50819	iu310604r_08071094051	6.9	2008-03-11	09:35:54.06	VISIR200	UV13	D	23K
50820	iu310605r_08071094051	11.0	2008-03-11	09:38:14.06	VISIR200	UV13	D	37K
50821	iu310607r_08071095828	15.4	2008-03-11	09:51:52.04	VISIR200	UV13	D	52K
50822	iu310608r_08071095828	18.7	2008-03-11	09:55:43.05	VISIR200	UV13	D	-15mm defocus
50823	iu31060ar_08071101833	112.0	2008-03-11	10:09:29.06	VISIR200	UV13	D	-15mm defocus
50824	iu31060br_08071101833	2.6	2008-03-11	10:16:06.06	VISIR200	UV14	B	9K

tvnum	image	exptime	date-obs	time-obs	source	field point	quadrant	comment
50825	iu31060dr_08071103432	6.9	2008-03-11	10:29:35.05	VISIR200	UV14	B	23K
50826	iu31060er_08071103432	11.0	2008-03-11	10:31:55.05	VISIR200	UV14	B	37K
50827	iu31060gr_08071105209	15.4	2008-03-11	10:45:33.06	VISIR200	UV14	B	52K
50828	iu31060hr_08071105209	18.7	2008-03-11	10:49:24.04	VISIR200	UV14	B	-15mm defocus
50829	iu31060jr_08071111214	112.0	2008-03-11	11:03:10.06	VISIR200	UV14	B	-15mm defocus
50830	iu31060kr_08071111214	2.6	2008-03-11	11:09:47.05	VISIR200	UV15	C	9K
50831	iu31060mr_08071112813	6.9	2008-03-11	11:23:16.04	VISIR200	UV15	C	24K
50832	iu31060nr_08071112813	11.0	2008-03-11	11:25:36.04	VISIR200	UV15	C	38K
50833	iu31060pr_08071114550	15.4	2008-03-11	11:39:14.06	VISIR200	UV15	C	53K
50834	iu31060qr_08071114550	18.7	2008-03-11	11:43:05.06	VISIR200	UV15	C	-15mm defocus
50835	iu31060sr_08071120554	112.0	2008-03-11	11:56:50.05	VISIR200	UV15	C	-15mm defocus
50836	iu31060tr_08071120554	2.6	2008-03-11	12:03:27.04	VISIR200	UV16	A	9K
50837	iu31060vr_08071122153	6.9	2008-03-11	12:16:56.06	VISIR200	UV16	A	23K
50838	iu31060wr_08071122153	11.0	2008-03-11	12:19:16.06	VISIR200	UV16	A	37K
50839	iu31060yr_08071123930	15.4	2008-03-11	12:32:54.05	VISIR200	UV16	A	51K
50840	iu31060zr_08071123930	18.7	2008-03-11	12:36:45.06	VISIR200	UV16	A	-15mm defocus
50841	iu310611r_08071125757	112.0	2008-03-11	12:50:31.04	VISIR200	UV16	A	-15mm defocus
50842	iu310612r_08071125757	0.0	2008-03-11	12:54:45.06	--	--	--	bias
50845	iu013a03r_08071142206	3000.0	2008-03-11	13:27:32.04	--	--	--	dark
50847	iu013a06r_08071151615	3000.0	2008-03-11	14:21:41.06	--	--	--	dark
50849	iu013a09r_08071161107	3000.0	2008-03-11	15:15:50.06	--	--	--	dark
52288	iu013a03r_08077163604	3000.0	2008-03-17	15:41:30.04	--	--	--	dark
52290	iu013a06r_08077173013	3000.0	2008-03-17	16:35:39.06	--	--	--	dark
52292	iu013a09r_08077182505	3000.0	2008-03-17	17:29:48.06	--	--	--	dark
55315	iu261301r_08091215817	1.0	2008-03-31	21:01:02	HeNe	UV01	straddle A/B	unsaturated, binned 3x3
55316 thru 55436	iu26133kr_08092043804 thru iu261302r_08091215817	25.0	2008-03-31	04:35:31 thru 21:03:56	HeNe	various	various	saturated, binned 3x3

Appendix B

Figure 4: Mosaic of 200x200 pixel subsections from images taken with the detector at nominal operating temperature, shown with an inverted greyscale stretch. Columns 1,3,5, and 7 show the target as it appeared in amps A, B, C, and D, respectively; the adjoining columns (2,4,6, and 8) show the resulting crosstalk in amps B, A, D, and C, respectively. The first four rows show the PSF at increasingly higher exposure levels, from about 8K e^- (row 1) up to >50K e^- (row4); the last two rows show the defocussed images taken at ~8K and ~45K e^- peak levels.

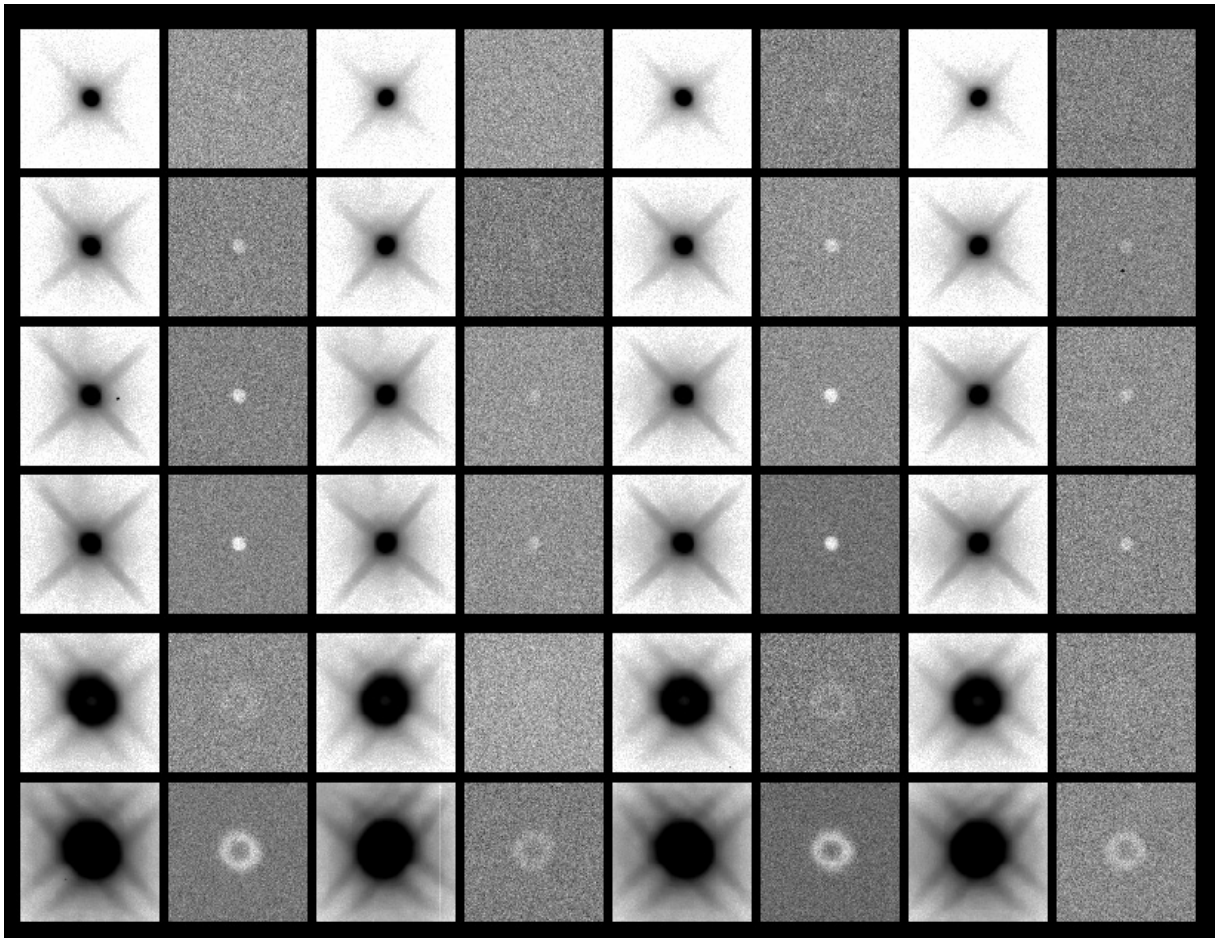

Figure 5: Mosaic of 100x100 pixel subsections from images taken with the detector at ambient temperature, shown with an inverted greyscale stretch. Columns 1,3,5, and 7 show the target as it appeared in amps A, B, C, and D, respectively; the adjoining columns (2,4,6, and 8) show the resulting crosstalk in amps B, A, D, and C, respectively. Images in the first row show an unsaturated point source target, as generated by the HeNe laser (about 30K e^- in the peak pixel). Images in the second row show a more extended target (200um point source, peak levels just at saturated, about 48K e-), and the third row is again a point source target at 100x the exposure level of the target in row 1.

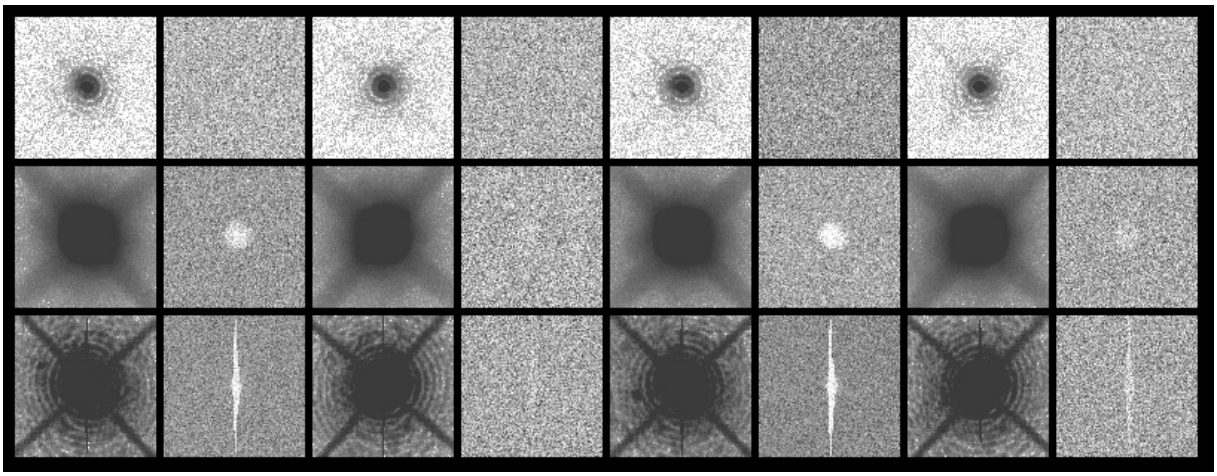

Figure 6: Mosaic of 100x100 pixel extracts from a subset of binned images taken with the detector at nominal operating temperature, shown with an inverted greyscale stretch. Targets in odd-numbered columns are in quadrants A, B, C, and D while images in even-numbered columns are the associated CT for each (i.e., quadrants B, A, D, and C).